The Astrophysical Journal, 782:94 (7pp), 2014 February 20 doi:10.1088/0004-637X/782/2/94

WHEN AND HOW DOES A PROMINENCE-LIKE JET GAIN KINETIC ENERGY?

Jiajia Liu, Yuming Wang[1], Rui Liu, Quanhao Zhang, Kai Liu, Chenglong Shen, and S. Wang
CAS Key Laboratory of Geospace Environment, Department of Geophysics and Planetary Sciences, University of Science & Technology of China, Hefei, Anhui 230026, China; ymwang@ustc.edu.cn
Received 2013 August 12; accepted 2014 January 2; published 2014 February 3

ABSTRACT

A jet is a considerable amount of plasma being ejected from the chromosphere or lower corona into the higher corona and is a common phenomenon. Usually, a jet is triggered by a brightening or a flare, which provides the first driving force to push plasma upward. In this process, magnetic reconnection is thought to be the mechanism to convert magnetic energy into thermal, nonthermal, and kinetic energies. However, most jets could reach an unusual high altitude and end much later than the end of its associated flare. This fact implies that there is another way to continuously transfer magnetic energy into kinetic energy even after the reconnection. The picture described above is well known in the community, but how and how much magnetic energy is released through a way other than reconnection is still unclear. By studying a prominence-like jet observed by *SDO*/AIA and *STEREO-A*/EUVI, we find that the continuous relaxation of the post-reconnection magnetic field structure is an important process for a jet to climb up higher than it could through only reconnection. The kinetic energy of the jet gained through the relaxation is 1.6 times that gained from the reconnection. The resultant energy flux is hundreds of times larger than the flux required for the local coronal heating, suggesting that such jets are a possible source to keep the corona hot. Furthermore, rotational motions appear all the time during the jet. Our analysis suggests that torsional Alfvén waves induced during reconnection could not be the only mechanism to release magnetic energy and drive jets.

Key words: magnetic reconnection – Sun: activity – Sun: filaments, prominences – waves

Online-only material: animations, color figures

1. INTRODUCTION

Solar jets are a ubiquitous activity in the solar atmosphere that occur in active, quiet Sun, and polar regions. According to their size and observed wavelengths, jets could be classified as surges (e.g., Newton 1934; Rust 1968; Roy 1973; Xu et al. 1984; Canfield et al. 1996; Jibben & Canfield 2004), multiwavelength (UV, EUV, X-ray) jets (e.g., Schmieder et al. 1988; Shibata et al. 1992; Cirtain et al. 2007; Culhane et al. 2007; Liu et al. 2009; Shen et al. 2011; Tian et al. 2012), and spicules (e.g., de Pontieu et al. 2007a, 2007b; Shibata et al. 2007). These jets carry lots of mass and energy from the low solar atmosphere into the corona and therefore are thought to play an important role in coronal heating and solar wind acceleration (e.g., Shibata et al. 1996, 2007; Tsiropoula & Tziotziou 2004; de Pontieu et al. 2007b).

Previous studies have shown that the length of solar jets range from about one to several hundred megameters, the speed could be from tens to thousands of kilometers per second, and the lifetime spreads from minutes to hours (e.g., Shibata et al. 1996; Cirtain et al. 2007; de Pontieu et al. 2007a). Usually, a jet has two components: a hot component and a cool component, which are mainly distributed in the temperature of the soft X-ray and 304 Å, respectively (e.g., Moore et al. 2013). Either component (hot or cool) could be dominant. Therefore, some jets are visible in Hα or 304 Å passbands, while some jets are visible in EUV or X-ray observations (e.g., Shen et al. 2011; Srivastava & Murawski 2011). Although different types of jets have different properties, some common phenomena could be found in most cases. The first common phenomenon is flaring, a manifestation of magnetic field reconnection. Except for Type I spicules (de Pontieu et al. 2007a), stronger or weaker flaring could be always found at the jet root. It is believed to be the initial and major driver of a jet. However, observations showed that the initial speed of a jet usually is too small to make it to a height as observed (e.g., Roy 1973; Liu et al. 2009; Shen et al. 2011), suggesting that some additional force after the flaring must act on the jet plasma.

This fact is closely related with another common phenomenon, which is the apparent rotational/torsional motion of jet plasma during its ascending and/or descending phase (e.g., Xu et al. 1984; Shibata & Uchida 1985; Canfield et al. 1996; Jibben & Canfield 2004; Shimojo et al. 2007; Liu et al. 2009). A well-accepted picture is that the reconnection between twisted loops and untwisted open field lines causes helicity to be transferred from loops to open field lines and therefore makes plasma move upward helically along the path by nonlinear torsional Alfvén waves (e.g., Pariat et al. 2009) or Lorentz force working (Shibata & Uchida 1985). It is interesting to see which one is more appropriate, or if there is alternative explanation.

One may find that the additional force pushing a jet unusually high is probably just the one driving the apparent rotational motion. In many cases, the jet keeps rising after reconnection. It implies that during a jet, the magnetic free energy is released through two different ways. One way is reconnection, and the other is post-reconnection relaxation of the magnetic field structure. Related to the issue raised for the rotational motion, an interesting question is how, and how significantly, the latter contributes to the jet kinetic energy, or in other words, when and how a jet gains its kinetic energy.

Here we will try to address this issue by investigating a prominence-like jet that was observed by *SDO*/AIA (Lemen et al. 2012) and *STEREO*/SECCHI EUVI (Howard et al. 2008) simultaneously. Thanks to the high-resolution, high-cadence, multiwavelength, and multipoint observations from *Solar Dynamics Observatory* (*SDO*) and *Solar TErrestrial RElations Observatory* (*STEREO*), we are for the first time able to accurately assess its energy budget in observations.

[1] Corresponding author.

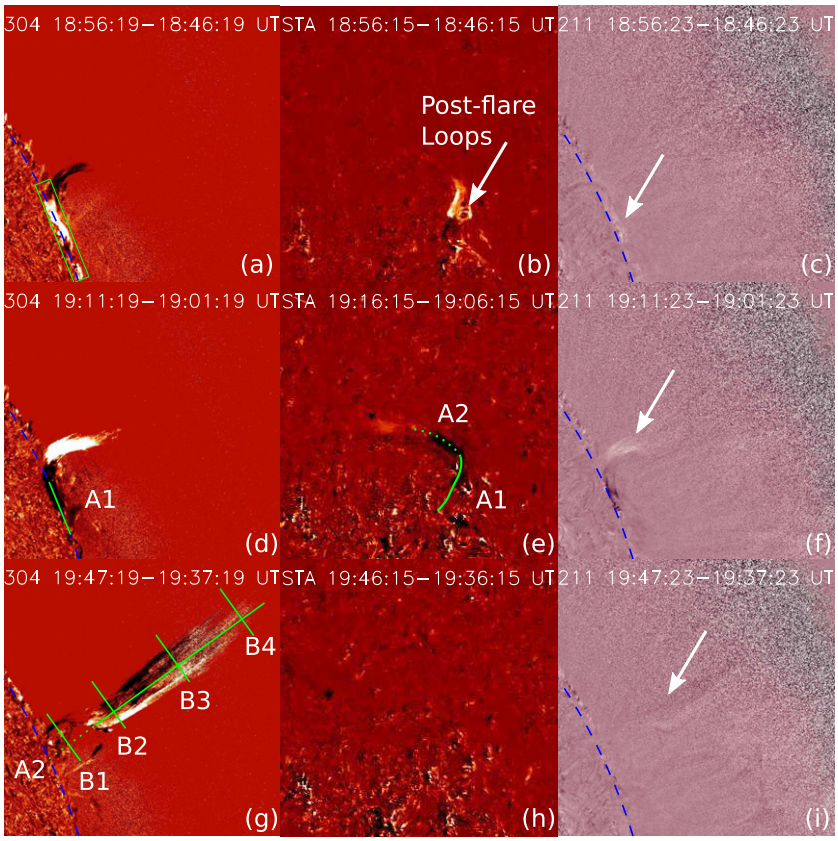

Figure 1. Left column: difference images taken by *SDO*/AIA at the 304 Å passband. The FOV of the images is 430″ × 430″. Middle column: difference images from *STEREO-A*/EUVI at the same passband. The FOV is 450″ × 450″. Since *STEREO-A* was 120° away from *SDO* on 2012 July 8, the *SDO* limb event on the right happened on the disk in the view of *STEREO-A*. Right column: difference images taken by *SDO*/AIA at the 211 Å passband with the same FOV as the images in the left column. The white arrow in the middle column denotes the post-flare loops and those in the right column mark the hot component of the jet.

(Animations and a color version of this figure are available in the online journal.)

2. OVERVIEW

The event is located off the northwest limb of the Sun, a bit north of the active region (AR) 11513. Two successive jets can be found at the same place from 18:00 to 21:00 UT on 2012 July 8 in various EUV passbands (see multiwavelength video 1). They were the most visible in 304 Å, and also showed weak signatures in the hotter channel 211 Å (as seen in Figure 1). But the jets were hard to see in emission lines with temperatures higher than 211 Å, suggesting that they are cool-component dominant jets with temperatures generally below 2 MK. Video 2 generated from the AIA 304 Å passband shows the detailed ejection process of the two jets. The first jet was a minor one with a lifetime of about one hour. It began to ascend at about 18:00 UT, reached its maximum height of about 90 Mm 35 minutes later, and then fell back to the solar surface at about 18:56 UT. The second jet is much more significant, which took place right after the first one and lasted for about 2 hr. In this study we will focus on the second jet.

The second jet was triggered by a microflare, which caused obvious enhancements of the EUV emissions at various wavelengths as shown in Figure 2, with the peak at about 19:01 UT (indicated by the black dashed line). The core of the microflare manifesting as a brightening point first appeared around 18:48 UT at the latitude of about 22° and then moved on the solar surface to the latitude of about 25°, which probably suggests that the reconnection point was moving. Meanwhile, several brightening small loops appeared beside the brightening point. Accordingly, some prominence-like materials traveled along a

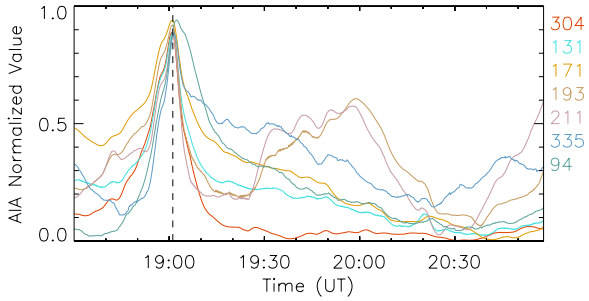

Figure 2. Normalized light curve derived from the integral emission from the brightening region (indicated by the green box in Figure 1(a)).

(A color version of this figure is available in the online journal.)

tunnel lying on the solar surface between the latitude of 22° and 25° at the beginning (see Figures 1(a) and (b)).

These materials formed the jet, which started to rise straightly at about 19:05 UT, slightly away from the local radial direction. According to Figure 2 and video 2, the microflare faded away around 19:11 UT, suggesting that the reconnection probably lasted for about 23 minutes. At that time, the jet was confined within a tunnel about 15 Mm wide (Figure 1(d)). The rising of the jet could be found in the *STEREO-A*/EUVI images (Figure 1(e)), but the signature is weak because of the relatively low resolution and low cadence of *STEREO* data.

The jet kept rising after 19:11 UT. It quickly expanded to about 35 Mm wide in a short distance and gradually grew to

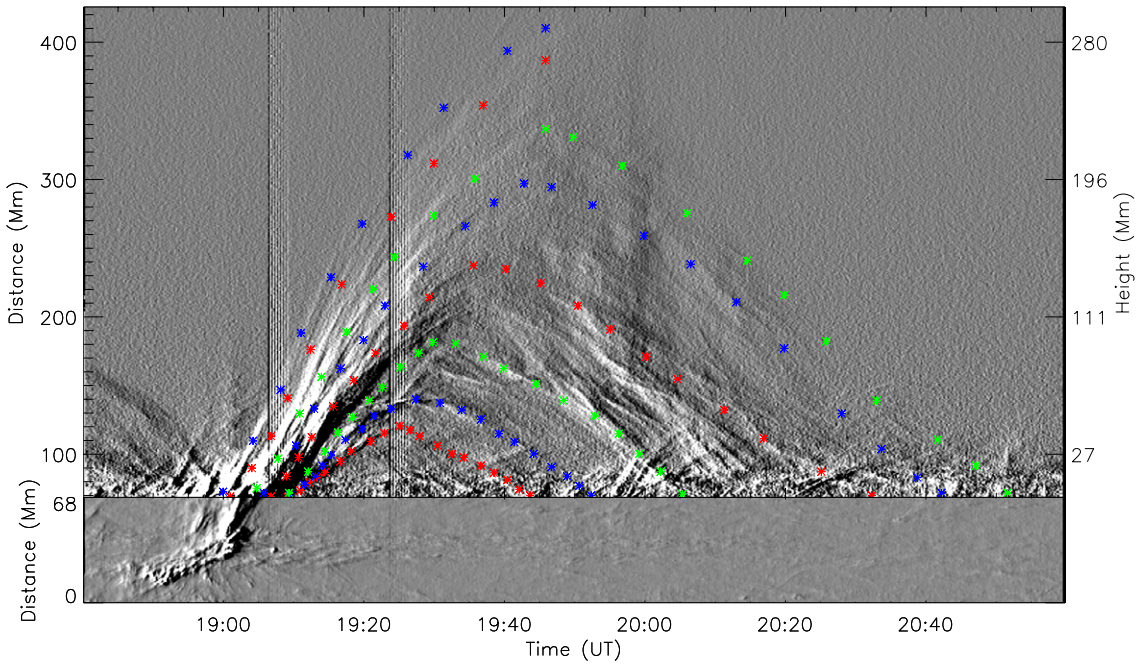

Figure 3. Lower part: deprojected running-difference space–time plot generated from slice A1 (see Figure 1(d)). Upper part: deprojected running-difference space–time plot generated from slice A2 (see Figure 1(g)). The left vertical axis gives the distance from the start point along the slice, and the corresponding height from the solar surface is marked on the right vertical axis.

(A color version of this figure is available in the online journal.)

about 50 Mm wide when it reached its maximum height of about 292 Mm at about 19:47 UT (Figure 1(g)). After then, the jet began to fall back. During the whole ejection process, we can find continuous rotational motion around the jet axis. From the AIA 304 Å movie, one can clearly distinguish many pieces of prominence-like materials rotating like a rigid object. In lots of previous studies, the rotational motion appeared only in the ascending phase. Thus, torsional Alfvén waves could be a driver of it. However, in this case, the jet plasma kept rotating during its descending phase, and the rotational period did not change significantly as will be seen in Section 4. This is difficult to explain with only an upward propagating wave train. This fact spurs us to figure out the real physics behind it. Is the rotational motion the manifestation of the real motion of plasma along twisted magnetic field lines or a rigid rotation of a bundle of untwisted magnetic field lines? To solve this puzzle, we analyze the axial motion and rotational motion, respectively, in the next two sections.

3. AXIAL MOTION

To study the axial motion of the jet, a slice is placed along the jet tunnel. The slice has two segments: one (labeled as A1 in Figure 1(d)) lies on the surface, and the other (A2, Figure 1(g)) stands upward straightly. The segment A1 was visible for both *SDO* and *STEREO-A* (solid green line in Figure 1(e)), and the projection effect could be easily removed. For segment A2, it is visible for *SDO* but not all for *STEREO-A*; only the lower part of A2 can be recognized in *STEREO-A*/EUVI images (as indicated by the dotted green line in Figure 1(e)). Thus, we assume that segment A2 is straight and use its lower part to correct the projection effect of A2. It is derived that the segment is about 30° away from the plane-of-sky in the view of *SDO*. A space–time plot generated from the slice is shown in Figure 3, in which the projection effect has been corrected.

An obvious acceleration could be seen in the plot when the jet moved on the surface. A quadratic fitting to the tracks in the low part of Figure 3 suggests that the acceleration is about 300 m s^{-2}. The jet moved with an average velocity of about 95 km s^{-1} and then turned upward with a speed of about 160 km s^{-1} overall. When the jet moved upward, we may distinguish many small sub-jets in it, which are shown as bright–dark alternating stripes in the upper part of Figure 3. These sub-jets were expelled successively. They experienced acceleration at the beginning and then turned to deceleration. We tracked eight sub-jets as indicated by the color-coded asterisks in Figure 3. The initial speeds of these sub-jets ranged from about 57 to 170 km s^{-1}, and through an acceleration, they reached maximum speeds in a range of about 79 to 238 km s^{-1} around 19:11 UT, when the brightening faded away. The earlier sub-jet has a larger acceleration and larger speed. These results are consistent with the fact that the microflare decayed with time.

After reaching the maximum upward speed, these sub-jets began to decelerate. Overall, the sub-jets were decelerated during the whole ascending phase, and the deceleration ranged from about −21 to −67 m s^{-2}. These values are smaller than the local gravity, even if the uncertainty (see the note in Table 1) is taken into account. It means that continuous upward force exists after the reconnection. These sub-jets finally reached up to a height from about 42 to 292 Mm (or 120 to 410 Mm in distance along the jet tunnel). Consistent with the speeds obtained before, the earlier sub-jets experienced a longer ascending phase and reached a higher height, which is clearly shown in Figure 3.

The descending speeds of these sub-jets were about −44 to −70 km s^{-1} with an average downward acceleration from −3 to −32 m s^{-2}, which were all smaller than those during the ascending phase. A direct consequence is that the duration of the descending phase is obviously longer than that of the ascending phase. Table 1 lists the kinematic parameters for the eight selected sub-jets.

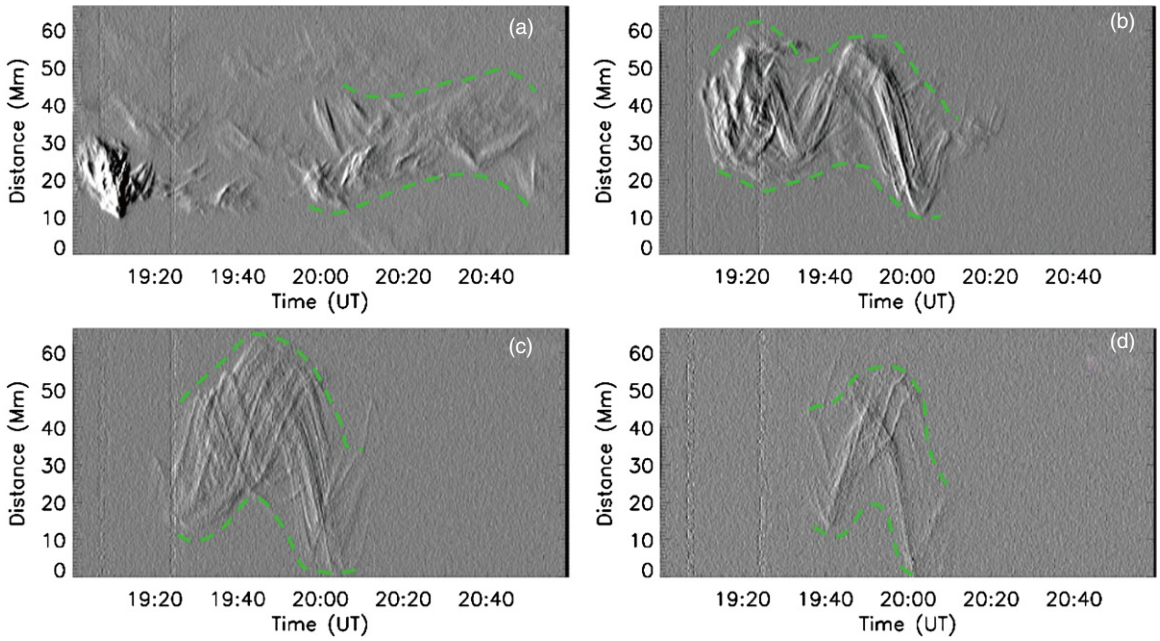

Figure 4. Running-difference space–time plot generated from slices B1, B2, B3, and B4, as marked in Figure 1(g). These four slices are all perpendicular to the jet's axis. Dashed lines indicate the boundary of the wriggling jet tunnel.

(A color version of this figure is available in the online journal.)

Table 1
Kinematic Parameters of Eight Sub-jets in the Axial Direction

Sub-jet	Ascending Phase					Descending Phase			H_{max}
	v_{ini}	v_{max}	v_{avg}	a_{avg}	T_a	v_{avg}	a_{avg}	T_d	
1	170 ± 10	238 ± 16	126 ± 2	-56 ± 5	2754	...	...	...	292
2	144 ± 14	193 ± 21	124 ± 2	-49 ± 5	2693	...	...	...	272
3	150 ± 12	178 ± 19	110 ± 2	-56 ± 6	2468	-70 ± 1	-6 ± 2	3943	229
4	140 ± 10	174 ± 18	102 ± 2	-48 ± 7	2222	-68 ± 1	-17 ± 3	3564	196
5	125 ± 19	135 ± 33	100 ± 3	-46 ± 12	1730	-53 ± 1	-3 ± 3	3340	145
6	104 ± 16	122 ± 30	90 ± 4	-35 ± 23	1229	-52 ± 2	-28 ± 8	2130	98
7	75 ± 24	126 ± 53	70 ± 5	-67 ± 31	1075	-49 ± 3	-32 ± 15	1495	61
8	57 ± 27	79 ± 50	56 ± 5	-21 ± 40	957	-44 ± 4	-10 ± 27	1106	42

Notes. Here v_{ini}, v_{max}, and v_{avg} are the initial, maximum, and average speed, respectively, in units of km s^{-1}; a_{avg} is the average acceleration in units of m s^{-2}; T_a and T_d are the duration in units of second; and H_{max} is the maximum height a sub-jet reached, which is units of Mm. The uncertainty in the velocity and acceleration is estimated through the fitting procedure by assuming a 10 pixel error in measuring height (corresponding to a 5 Mm error in distance). Positive values correspond to the upward direction.

4. ROTATIONAL MOTION

In order to analyze the rotational motion of the jet, we place four slices perpendicular to the jet tunnel at the height of 30, 90, 180, and 270 Mm, respectively (marked by B1 to B4 in Figure 1(g)). Figure 4 shows the space-time plots generated from the four slices, in which the end of a slice at the higher latitude is referred as zero and stripes with positive slopes indicate motion of material from higher latitude toward lower latitude.

From these plots, we can see many sine-like tracks, suggesting rotational motion in the jet tunnel. Such sine-like tracks appeared during both ascending and descending phases. In particular, these rotating materials seemingly concentrated near the surface of the jet tunnel. According to these tracks, we find that the jet tunnel was wriggling slightly, as indicated by the dashed lines. It is estimated that the width of the jet tunnel at the four heights is about 12, 30, 40, and 45 Mm, respectively.

Assuming that the jet tunnel is a cylinder with a varying radius, the real rotational speed could be derived by fitting these curves with a sine function. Table 2 gives the derived parameters for the rotational motion. It is found that their period is around 1270 s, and there is no significant difference in the period at different heights. The real rotational speed at the four different heights is therefore about 32, 74, 97, and 106 km s^{-1}, respectively. Although these results suffer from a large error,

Table 2
Kinematic Parameters of the Rotational Motion of the Jet

	H	D	T_c	v_ϕ
B1	30	12	1180 ± 120	32 ± 3
B2	90	30	1270 ± 230	74 ± 13
B3	180	40	1290 ± 330	97 ± 25
B4	270	45	1330 ± 250	106 ± 20

Notes. Here H is the height of the four slices in units of Mm, D is the width (diameter) of the jet tunnel in units of Mm, T_c is the period of the rotational motion in units of seconds, and v_ϕ is the rotational speed in units of km s^{-1}.

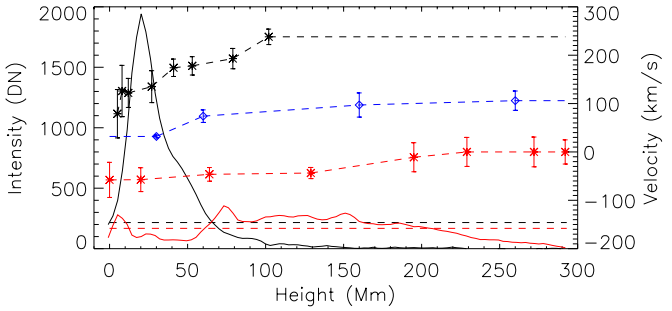

Figure 5. Solid lines show the integrated intensity of EUV 304 Å emission over the cross section of the jet as a function of height, in which the background emission is subtracted. The black line is calculated at 19:11 UT and the red line at 19:47 UT. The mean intensity at the two instants is indicated by two horizontal dashed lines, which are very close to each other. Asterisks connected with dashed lines indicate the axial velocities of the eight sub-jets, and the diamonds connected with dashed lines are the rotational velocities at the four heights.

(A color version of this figure is available in the online journal.)

they suggest that the jet material rotated faster and faster as it ascended and then slowed down when it fell back.

As mentioned before, for such an apparent rotational motion, there could be two different interpretations. One is that prominence-like materials move along twisted or helical magnetic field lines, and the other is that a bundle of straight magnetic field lines rotate as a rigid body in which prominence-like materials move up and down. If the first interpretation is the case, we expect that the turns the materials rotated around the jet tunnel within a given distance should be the same for different sub-jets. For sub-jet 1 (see Table 1), the turns per unit length is $n = (1/T_c v_{\rm avg}) \approx 1/(1270({\rm s}) \times 126\ ({\rm km\ s^{-1}})) = 0.006\ {\rm Mm^{-1}}$. Using this number to constrain sub-jet 7 or 8, we may derive that the expected period of them should be about 2381 or 2976 s, which is much larger than the observed period given in Table 2 even if the uncertainty is taken into account, and it cannot be found in the space-time plots.

Thus, the second interpretation is more appropriate. In this scenario, the jet tunnel above the limb consists of straight/untwisted open magnetic field lines. They rotated because of the reconnection at the jet root, which connected the untwisted open magnetic field lines to a bunch of highly twisted magnetic field loops and caused the helicity transported from the twisted fields into untwisted fields. The brightening and small loops shown in the first and second panels of Figure 1 are the signatures. The transport process therefore manifested a rotational motion.

5. ENERGY BUDGET

During the jet process, some prominence-like materials reached as high as 290 Mm or so, suggesting a significant release of magnetic energy. The release process of the magnetic energy obviously has two stages. The first stage is from 18:48 to 19:11 UT. During the stage, a microflare took place and then faded away, and meanwhile, the jet traveled on the solar surface and then climbed up to as high as 100 Mm. The second stage is from 19:11 UT to the end of the event. During the stage, the jet continuously ascended until about 19:47 UT and then fell back. The acceleration is significantly smaller than the solar gravity.

For most of such events, the magnetic energy was released through two ways. One way is through the magnetic reconnection, during which the free magnetic energy is directly converted to produce both thermal and nonthermal emissions and kinetic energy of plasma jets. The resultant magnetic structure through the reconnection may not be at a stable state. It will further relax its configuration to a lower energy level. This becomes the other way to release the free energy. For the first stage, both ways may take effect, and for the second stage, the second way is the only one. It is not new for us that the magnetic energy could be released in such ways, but it is unclear whether only one of them or both are important for the ejecta. A flare is much easier to see and is usually thought to be the major approach to convert magnetic energy into plasma kinetic energy. How much magnetic energy will be further released after a flare? This question is now be addressed below.

Table 3
Energies of the Jet at Two Instants

Time	E_g	E_l	E_a	E_t
19:11 UT	0.88	$1.15^{+0.44}_{-0.35}$	$0.11^{+0.03}_{-0.04}$	$2.14^{+0.47}_{-0.39}$
19:47 UT	2.83	$0.08^{+0.08}_{-0.04}$	$0.37^{+0.18}_{-0.14}$	$3.28^{+0.26}_{-0.18}$

Note. Energies are in units of 10^{10} J kg^{-1}.

Here we compare two instants. One is at 19:11 UT when the microflare ended and the jet roughly reached a maximum ascending speed (Figure 1(d)), and the other is at 19:47 UT when the jet reached the maximum height (Figure 1(g)). Figure 5 shows the emission intensity, I, as a function of the height at the two instants. The emission intensity is calculated on the basis of images in the EUV 304 Å passband, and it is an integrated value over the cross section of the jet cylinder at any given height. Here the background emission is removed by subtracting the average value of the pixels surrounding the jet.

The average value I_0 of the intensity of the whole jet is about 216 and 168, respectively, in units of digital number (DN) at the two instants (as indicated by the two horizontal dashed lines in Figure 5). For prominences observed in the 304 Å emission line, which is optically thick, it could be accepted that $\rho \propto I$, where ρ is the density. Thus, the product of the average intensity and the height could be a proxy of the mass of the jet material. The difference of the average intensity between the two instants suggests that the mass is not the same, but the difference is relatively small. It may be caused by the errors in measurements or the shielding effect in the optically thick medium.

In order to make the two instants comparative, we investigate the energy per unit mass. According to the distribution of the intensity shown in Figure 5, the gravitational potential energy per unit mass gained by the jet can be calculated by $E_g = GM_\odot(\int_0^H I(1/R_\odot - 1/(h+R_\odot))dh/\int_0^H Idh)$. The kinetic energy per unit mass of the jet consists of two components. One component is the linear kinetic energy, and the other is the angular kinetic energy, which are given by $E_l = (\int_0^H iv^2 dh/2\int_0^H Idh)$ and $E_a = (\int_0^H iv_\phi^2 dh/2\int_0^H Idh)$. The linear velocity could be read from Figure 3 and the angular velocity from Table 2. These velocities have been marked as symbols in Figure 5. The velocity between the symbols is obtained by using linear extrapolation, and the velocity outside the symbols just chooses the value of the nearest symbol (as indicated by the dashed lines connecting the symbols).

Table 3 lists the energies per unit mass. First of all, the total energy at 19:47 UT is larger than that at 19:11 UT. Their difference ΔE is about 1.14×10^{10} J kg^{-1}, which is about three times the uncertainties of the total energy at each instant, suggesting a significant difference. The microflare ended at 19:11 UT, which means that there was a continuous conversion

from magnetic energy to potential and kinetic energies after the reconnection. The observed rotational motion suggests that an untwisting process at the root of the jet is responsible for the energy conversion, through which the post-reconnection magnetic field structure relaxes to a lower energy state. The amount of the released magnetic energy could be alternatively estimated from the measurements of the accelerations of sub-jets. Since their acceleration (see $a_{\rm avg}$ listed in Table 1) is much smaller than the gravity, there must be additional force $f = m(a_{\rm avg} - g)$ acting on the jet, where m is the mass and $g = -274$ m s^{-2} is the gravity. The work per unit mass done by the force is $W = fH/m = (a_{\rm avg} - g)H$. According to the values of $a_{\rm avg}$ and H given in Table 1, it is easily inferred that W is on the order of 10^{10} J kg^{-1}, which is consistent with ΔE derived above.

Usually, reconnection produces straight plasma beams, like a jet. Thus, it is reasonable to assume that the angular kinetic energy E_a should mostly come from the untwisting process. We may infer that for the kinetic energy (including the potential energy) of the jet, the contribution from the reconnection, i.e., the microflare, is $E_r = E_{t0} - E_{a0} = 2.03 \times 10^{10}$ J kg^{-1} and the contribution from the untwisting process in the ascending phase is $E_{ua} = E_{t1} - E_{t0} + E_{a0} = 1.25 \times 10^{10}$ J kg^{-1}, where the subscripts 0 and 1 refer to the instant of 19:11 and 19:47 UT, respectively. Moreover, by considering that (1) the rotational motion continuously existed during the descending phase, (2) the rotational velocity and period are almost as the same as those during the ascending phase, and (3) the duration of the descending phase is about 1.57 times that of the ascending phase (Table 1), we derive that the contribution of the untwisting process during the whole event is roughly $E_u = 2.57E_{ua} = 3.2 \times 10^{10}$ J kg^{-1}, which is 1.6 times the kinetic energy that could be injected by the reconnection. Even if considering the kinetic energy produced by a reconnection/flare is only a small fraction (about 10%) of its total released energy (e.g., Woods et al. 2004; Benz 2008; Reeves et al. 2010; Emslie et al. 2012), the contribution of the untwisting process is still significant, which is about 16% of the total released magnetic free energy by a reconnection.

6. CONCLUSIONS AND DISCUSSIONS

We presented the observational features of a prominence-like jet event observed by *SDO*/AIA and *STEREO*/SECCHI EUVI simultaneously on 2012 July 8. Like most jets observed before, it was triggered by a microflare accompanied with several small brightening loops, suggesting a weak reconnection. After obtaining initial momentum, the jet traveled along a tunnel to reach a height of about 292 Mm above the solar surface and then returned back to the Sun. During the whole process, the acceleration in radial direction is significantly smaller than solar gravity, implying an additional force acting on the jet plasma even after the reconnection. All these observations fit well the classical jet model as proposed in Figure 4 of the paper by Shibata et al. (1996).

The magnetic free energy is released through two ways during the jet. One way is reconnection, and the other is the magnetic field relaxation after the reconnection. By analyzing its motion and energy budget, we find that the magnetic field relaxation after the reconnection makes a significant contribution for the jet to gain kinetic energy, which is about 1.6 times the contribution made by reconnection and about 16% of the total magnetic free energy that could be released by the reconnection.

Rotational motion is a manifestation of the continuous conversion of magnetic energy into kinetic energy through a way other than the reconnection. In this case, we believe that the twisted loops, which are connected to the untwisted magnetic field lines, drive the rotation. But different from the traditional picture, the rotation is probably not mainly caused by torsional Alfvén waves (Pariat et al. 2009). The reason is that (1) the rotation appeared in both ascending and descending phases and (2) the additional force preventing the jet plasma falling back is even larger during the descending phase, which caused the descending phase to be much longer than the ascending phase. These new findings are not expected by the classical jet model. What the physics are behind them is worthy of further study.

A similar picture showing the rotation of a bundle of untwisted (or weak twisted) magnetic field lines could be found in a recent study of solar tornadoes/cyclones (Wedemeyer-Böhm et al. 2012). In their case, vortex flows at the base rather than reconnection driving up flow. Solar cyclones are found to be a ubiquitous phenomenon in the solar atmosphere (e.g., Brandt et al. 1988; Wedemeyer-Böhm & Rouppe van der Voort 2009; Attie et al. 2009; Zhang & Liu 2011; Wedemeyer-Böhm et al. 2012; Li et al. 2012; Liu et al. 2012; Su et al. 2012). Jets are also a ubiquitous phenomenon in the solar atmosphere. Thus, we may conjecture that the rotational motion generated during jets, which is usually observed from the side view, and the cyclones that are usually observed from the top view may probably be the same thing, or at least jets are a subset of solar cyclones. For this case, we are unable to make a deeper analysis on this issue because of the low resolution and low cadence of *STEREO-A* data, although *STEREO-A* observed the event from another angle of view.

In this case, the conversion rate per unit mass of the magnetic energy to kinetic energy is about $E_u/(T_a + T_d) = 5 \times 10^6$ J kg^{-1} s^{-1}. By assuming a typical number density of about 10^{10} cm^{-3} of the jet plasma (Roy 1973), the conversion rate per unit volume is about 8×10^{-5} J m^{-3} s^{-1}, and the momentum flux is about 1.7×10^4 J m^{-2} s^{-1} by considering a length scale of about 200 Mm. The radiation of the hot corona requires an energy flux of about 3×10^2 J m^{-2} s^{-1} into thermal energy (e.g., Withbroe and Noyes 1977; Aschwanden 2006), which is 2% of the momentum flux of the jet. In other words, the local corona could be heated as long as only a very small fraction of kinetic energy carried by the jet is dissipated. Thus, we believe that jets are able to heat local corona when they get kinetic energy, as suggested in many previous studies for spicules and X-ray jets (e.g., Tsiropoula & Tziotziou 2004; de Pontieu et al. 2007b; Shibata et al. 2007; Cirtain et al. 2007).

We acknowledge the use of data from the AIA instrument on board *Solar Dynamics Observatory* (*SDO*) and EUVI instrument on board *Solar TErrestrial RElations Observatory* (*STEREO*). This work is supported by grants from the CAS (the Key Research Program KZZD-EW-01-4, 100-talent program, KZCX2-YW-QN511, and startup fund), 973 key project (2011CB811403), NSFC (41131065, 40904046, 40874075, and 41121003), MOEC (20113402110001), and the fundamental research funds for the central universities.

REFERENCES

Aschwanden, M. J. 2006, Physics of the Solar Corona—An Introduction with Problems and Solutions (Chichester, UK: Springer)
Attie, R., Innes, D. E., & Potts, H. E. 2009, A&A, 493, L13
Benz, A. O. 2008, LRSP, 5, 1

Brandt, P. N., Scharmer, G. B., Ferguson, S., Shine, R. A., & Tarbell, T. D. 1988, Natur, 335, 238
Canfield, R. C., Reardon, K. P., Leka, K. D., et al. 1996, ApJ, 464, 1016
Cirtain, J. W., Golub, L., Lundquist, L., et al. 2007, Sci, 318, 1580
Culhane, L., Harra, L. K., Baker, D., et al. 2007, PASJ, 59, S751
de Pontieu, B., McIntosh, S., Hansteen, V. H., et al. 2007a, PASJ, 59, 655
de Pontieu, B., McIntosh, S. W., Carlsson, M., et al. 2007b, Sci, 318, 1574
Emslie, A. G., Dennis, B. R., Shih, A. Y., et al. 2012, ApJ, 759, 71
Howard, R. A., Moses, J. D., Vourlidas, A., et al. 2008, SSRv, 136, 67
Jibben, P., & Canfield, R. C. 2004, ApJ, 610, 1129
Lemen, J. R., Title, A. M., Akin, D. J., et al. 2012, SoPh, 275, 17
Li, X., Morgan, H., Leonard, D., & Jeska, L. 2012, ApJL, 752, L22
Liu, J., Zhou, Z., Wang, Y., et al. 2012, ApJL, 758, L26
Liu, W., Berger, T. E., Title, A. M., & Tarbell, T. D. 2009, ApJL, 707, L37
Moore, R. L., Sterling, A. C., Falconer, D. A., & Robe, D. 2013, ApJ, 769, 134
Newton, H. W. 1934, MNRAS, 94, 472
Pariat, E., Antiochos, S. K., & DeVore, C. R. 2009, ApJ, 691, 61
Reeves, K. K., Linker, J. A., Mikić, Z., & Forbes, T. G. 2010, ApJ, 721, 1547
Roy, J.-R. 1973, SoPh, 32, 139
Rust, D. M. 1968, in IAU Symp. 35, Structure and Development of Solar Active Regions, ed. K. O. Kiepenheuer (Dordrecht: Reidel), 77
Schmieder, B., Simnett, G., Tandberg-Hanssen, E., & Mein, P. 1988, A&A, 201, 327
Shen, Y., Liu, Y., Su, J., & Ibrahim, A. 2011, ApJL, 735, L43
Shibata, K., Ishido, Y., & Action, L. W. 1992, PASJ, 44, L173
Shibata, K., Nakamura, T., Matsumoto, T., et al. 2007, Sci, 318, 1591
Shibata, K., Shimojo, M., Yokoyama, T., & Ohyama, M. 1996, in ASP Conf. Ser. 111, Theory and Observations of X-Ray Jets, ed. R. D. Bentley & J. T. Mariska (San Francisco, CA: ASP), 29
Shibata, K., & Uchida, Y. 1985, PASJ, 37, 31
Shimojo, M., Narukage, N., Kano, R., et al. 2007, PASJ, 59, S745
Srivastava, A. K., & Murawski, K. 2011, A&A, 534, A62
Su, Y., Wang, T., Veronig, A., Temmer, M., & Gan, W. 2012, ApJL, 756, L41
Tian, H., McIntosh, S. W., Xia, L., He, J., & Wang, X. 2012, ApJ, 748, 106
Tsiropoula, G., & Tziotziou, K. 2004, A&A, 424, 279
Wedemeyer-Böhm, S., & Rouppe van der Voort, L. 2009, A&A, 507, L9
Wedemeyer-Böhm, S., Scullion, E., Steiner, O., et al. 2012, Natur, 486, 505
Withbroe, G. L., & Noyes, R. W. 1977, ARA&A, 15, 363
Woods, T. N., Eparvier, F. G., Fontenla, J., et al. 2004, GeoRL, 31, L10802
Xu, A., Ping, D., & Yin, S. 1984, AcASn, 25, 119
Zhang, J., & Liu, Y. 2011, ApJL, 741, L7